Rev. Int. Contam. Ambie. 38 (Environmental Science and Policy for Sustainable Development) 1-12, 2022
https://doi.org/10.20937/RICA.54615

MECHANICAL PROPERTIES OF CONCRETE AFTER ACID RAIN CORROSION BASED ON PARTICLE DISCRETE ELEMENT

Propiedades mecánicas del hormigón corroído por la lluvia ácida con base en el elemento discreto de partículas

Guang YANG and Guoxin LI*

College of Materials Science and Engineering, Xi'an University of Architecture and Technology, Xi'an 710055, China.

* Author for correspondence: yangguang254@163.com

(Received: October 2021; accepted April 2022)

Key words: Particle discrete element, concrete, acid rain, corrosion, mechanical properties.

ABSTRACT

To predict the durability of concrete structure and ensure the safety of life and property, a method to analyze the mechanical properties of concrete corroded by acid rain based on particle discrete element is presented. Eight test specimens of prestressed concrete beams were designed, and then test specimens of concrete beams with different corrosion rates were obtained by simulation of acid rain corrosion. The impact splitting load test was carried out based on the particle discrete element, and then the meso-mechanics model of concrete particle discrete element was built. Experiment results show that the stress process of the test concrete beam after acid rain corrosion includes three stages: uncracking, crack increasing with load, crushing and spalling. After the acid rain corrosion, the splitting tensile strength of TYL-b (the upper tensile reinforcement) beam is the highest, and the splitting tensile strength of TYL-d (the lower compression reinforcement) beam is the lowest. The corrosion rate of acid rain is inversely proportional to the splitting tensile strength of concrete. The splitting tensile strength of concrete after acid rain corrosion obtained by the proposed method is consistent with the actual value. Therefore, the proposed method has high accuracy and high practical value.

Palabras clave: elemento discreto de partículas, lluvia ácida, corrosión, propiedades mecánicas.

RESUMEN

Para predecir la durabilidad de la estructura de hormigón y garantizar la seguridad de la vida y la propiedad, se presenta un método para analizar las propiedades mecánicas del hormigón corroído por la lluvia ácida con base en el elemento discreto de partículas. Se diseñaron ocho muestras de prueba de vigas de hormigón pretensado, y luego se obtuvieron muestras de prueba de vigas de hormigón con diferentes tasas de corrosión mediante la simulación de la corrosión por lluvia ácida. La prueba de división de impacto se llevó a cabo con base el elemento discreto de partículas y luego se construyó el modelo mesomecánico de elemento discreto de partículas de hormigón. Los resultados del experimento muestran que el proceso de estrés de la viga de hormigón de prueba después de la corrosión por lluvia ácida incluye tres etapas: desmonoramiento, aumento de la grieta por la carga, trituración y astillado. Después de la corrosión por lluvia ácida, la resistencia a la tracción de división del haz TYL-b (el refuerzo de tracción superior) es la más alta, y la resistencia a la tracción de división del haz TYL-d (el refuerzo de compresión inferior) es la más baja. La tasa de corrosión de la lluvia ácida es inversamente proporcional a la resistencia a la tracción de división del hormigón. La resistencia a la tracción por hendimiento del hormigón después de la corrosión por lluvia ácida obtenida por el método propuesto es coherente con el valor real. Por lo tanto, el método propuesto tiene una alta precisión y un alto valor práctico.

INTRODUCTION

At present, the prestressed concrete technology is widely applied in high-rise buildings, underground buildings, high-rise structures, hydraulic buildings, marine structures, airport runways, pressure vessel of nuclear power plants and large tonnage ships. In general, the durability of prestressed concrete is better than ordinary reinforced concrete, but the function of prestressed concrete structure will gradually decline in long-term use (such as chemical medium erosion, freeze-thaw and carbonation). The prestressed steel (steel strand) is always high stress state in the component, and it is highly sensitive to the corrosion environment. Once the steel strand breaks due to stress corrosion, the engineering accidents may occur without warning, and the harm to social economy and safety is far greater than the ordinary reinforced concrete structure damage (Chen et al. 2021b, Michael et al. 2016). China has become the third acid rain area in the world. The sulfate ion in acid rain reacts with the hydration product of cement to produce the product with expansion failure, and thus to increase the corrosion rate of prestressed reinforcement.

At present, the three-dimensional numerical mechanical simulation of concrete mainly uses the finite element method for analysis. The essence of finite element calculation is to calculate the continuous area change of the similar displacement field through the finite element model and output the calculation results. The essence of cracks is the non-uniformity and non-continuity of concrete material. This makes the finite element method more difficult to simulate the material failure and cracking. Granular materials are very common in nature and engineering, which are divided into particles and powders (Zohdi, 2016). Its mechanical characteristics can be summarized as “dispersion” and “motion”. In the past, the theory of continuum mechanics was often used to analyze the process of dispersion, leading to the deviation between theory and practice. With the development of computational technology, the discrete element method (Discrete/Distinct Element Method, DEM) has emerged in the field of granular mechanics.

The particle discrete element method is an effective tool that is specially used to study the micromechanical behavior of granular materials. This method has advantages in processing the granular materials and micro cracks (Hao et al. 2017, Kaianauskas et al. 2015). Chen et al. (2020) proposed a method to simulate the static performance of concrete filled steel tubular (CFST) members under acid rain corrosion. The influence of corrosion rate on yield strength, elastic modulus, ultimate tensile strength and ultimate elongation of steel was analyzed. Combined with the finite element Abaqus software, the load-deformation relation curve of the component is calculated respectively, and the ultimate bearing capacity is not good. Three E1 seismic waves and three E2 seismic waves are generated by Matlab programming, which are consistent with the response spectrum of the actual bridge site, and the dynamic time-history analysis is carried out for the piers under different corrosion rates. This method can analyze the mechanical properties of the pier under the load, but its accuracy is not high (Zhang et al. 2020).

In view of the poor accuracy of traditional methods, this paper proposes an analysis method based on particle discrete element to analyze the influence of concrete mechanical properties after acid rain corrosion, and obtains the changes of concrete mechanical properties under different degrees of acid rain corrosion. The splitting tensile strength results of each test beam obtained by this method are very close to the actual value, indicating that this method has high accuracy and the analysis results are in line with the actual situation. It can be used to analyze the influence of concrete mechanical properties after acid rain corrosion, and has high practical application value. It provides an effective basis for judging and predicting the service life of various construction projects in advance, avoiding engineering accidents, and ensuring the safety of people’s lives and property.

MATERIAL AND METHOD

Test materials

The P·O42.5 cement produced by Jiangxi Ganjiang Cement Plant was used in the test, and the Cement of H65 type was P·O52.5. Fine aggregate is made locally in Ganjiang River, with a fineness modulus of 2.5. Coarse aggregate is made of crushed stone with continuous gradation of 5-25 mm. The strength grade and mixing ratio of concrete are listed in **Table I**.

TABLE I. CONCRETE MIX RATIO.

Strength grade	H45	H55	H65
Fine aggregate/kg/m^3	578	519	503
The aggregate/ kg/m^3	1185	1169	1187
Cement/ kg/m^{33}	402	464	455
Water/ kg/m^{33}	172	179	179
The measured intensity/(MPa,GPa)	43.4	50.1	58.8

Eight prestressed concrete rectangular beams were designed in the experiment. φ^s15.2 (1 × 7) 1860 steel strand was adopted. The yield strength is 1661 MPa. The ultimate strength is 1931 MPa and the modulus of elasticity is 202 GPa. The elongation is 5.6%. The static splitting tensile strength is 2.69 MPa. The peak load is 8.6 kN. The static uniaxial compressive strength is 25.0 MPa. The uniaxial compressive strength of standard cube is 21.0 MPa. The reinforcement is HRB400 grade, the thickness of protective layer a_s = 40 mm. The reinforcement arrangement is shown in **figure 1**.

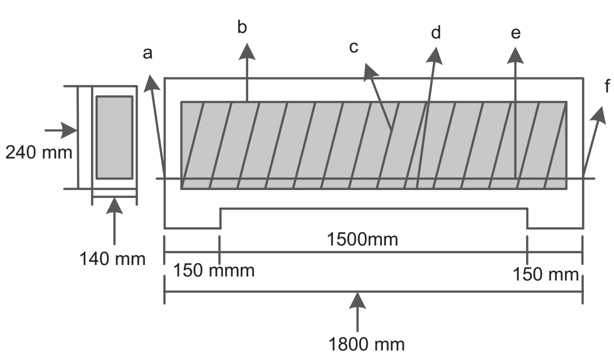

Fig. 1. Overall specimen design.

Design of test specimen

Three factors (concrete strength, prestressing force and corrosion rate of steel strand) are taken as the variable parameters, and eight test specimens of post-tensioned prestressed concrete beams are made by steel pipe core-pulling method.

The concrete strength is designed as H45, H55 and H65 respectively. At present, the concrete beam with moderate prestressing force is commonly used in the project. In order to conform to the actual situation of project the prestressing force PPR is controlled in the moderate force (0.55 ≤ PPR≤ 0.75). The prestressed concrete beam is corroded by electrified accelerated immersion. The size of test specimen is 140 mm × 240 mm × 2000 mm. The detailed parameters are listed in **table II** and **figure 1**.

Note: The prestressing force PPR = $A_pf_{py}/(A_pf_{py}+A_sf_y)$. A_p is the area of prestressed reinforcement and A_s is the area of tensile reinforcement. f_{py} is the design value of tensile strength of prestressed reinforcement and $f_y$is the yield strength of tensile reinforcement.

Note: a. is the backing board; b. is the upper tensile reinforcement; c. is the hooping (diameter 8 mm); d. is the lower compression reinforcement; e. is the prestressed reinforcement; f. is the single hole anchorage.

Experimental method

Test of acid rain corrosion

First, simulate acid rain erosion. In view of the influence of acid rain corrosion on the mechanical properties of concrete, this paper adopts the simulated acid rain alternate dry and wet test method. The test device is shown in **figure 2**. The test steps are as follows:

The eccentrically loaded reinforced concrete column was taken out and the two ends of the specimen were treated with epoxy resin. After drying, the specimens (including prismatic concrete specimens) were immersed in water or simulated acid rain, and then corroded alternately in wet and dry cycles (Aqsa 2020, Aunsary and Chen 2019, Kang et al. 2018). The dry and wet alternate cycle system is as follows: The specimen is soaked in solution for 1 day, and then naturally dried for 1 day at about 25 ºC, that is, one cycle. Soak in the process, every day with PS-II acidity meter, real-time monitoring solution pH value change, if the solution is dilute nitric acid, is used to adjust to the original acidity, every two dry-wet alternate cycle change one solution.

When the dry and wet cyclic corrosion of the test specimen in solution reaches the predetermined corrosion time (T), the specimen is taken out and dried, and then the eccentrically loaded bearing capacity

TABLE II. SPECIMEN PARAMETERS.

Specimen number	TYL-a	TYL-b	TYL-c	TYL-d	TYL-e	TYL-f	TYL-g	TYL-h
Concrete strength grade	H55	H55	H55	H55	H55	H55	H65	H45
Ordinary steel bar in tensile area	2φ11	2φ11	2φ11	2φ11	2φ13	2φ15	2φ13	2φ11
Common reinforcement in compression zone	2φ11	2φ11	2φ11	2φ11	2φ11	2φ11	2φ11	2φ11
Prestressed degree	0.56	0.56	0.56	0.56	0.49	0.43	0.56	0.56
Corrosion rate of steel strand/%	4	0	7	10	7	7	7	7

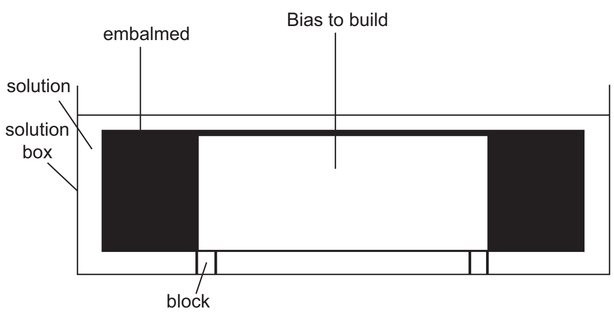

Fig. 2. Diagram of test apparatus.

test of reinforced concrete, compressive strength of concrete axis, elastic modulus and acid rain acidification depth test are carried out. According to the typical ions and acidity composition of Chinese acid rain, concentrated sulfuric acid, ammonium sulfate and magnesium sulfate were used to simulate acid rain. However, in order to speed up the corrosion rate, partial ion concentration was increased in this paper, and acid rain acidity pH 1, pH 2 and pH 3 were three cases. The composition of other ions is shown in **table III**. It should be noted that in the simulation of acid rain erosion in this paper, the ambient temperature is not controlled, but the room temperature at that time shall prevail.

TABLE III. MAIN IONIC CHEMICAL COMPOSITION OF SIMULATED ACID RAIN (mol/L).

Composition	SO_4^{2-}	NO^{3-}	Mg^{2+}	NH^{4+}	Ca^{2+}
Content	0.01	0.15	0.002	0.002	0.001

The indoor accelerated corrosion was used to study the prestressed concrete beams. After the members were maintained for 28 days, the prestressed reinforcement was tensioned. After the tensioning, the members were put into the acid rain solution for accelerated corrosion.

The method of electrified accelerated corrosion was adopted. In order to prevent the current from being too large, the DC stabilized voltage power supply was adopted, and the current density was controlled at less than 300 $\mu A/cm^2$. In this experiment, the accelerated corrosion current density was 200 $\mu A/cm^2$, reaching the expected corrosion rate of steel strand. The corrosion days were 30 days, 60 days and 90 days. The DC regulated power supply is shown in **figure 3**.

Fig. 3. DC stabilized power supply device.

According to the analysis of rainfall composition in recent 10 years of Nanchang, the composition of simulated acid rain solution was obtained. According to the change of rainfall pH value, the pH value of solution was set as 2.3. Ammonium sulfate 0.132 g, magnesium sulfate 0.24 g, sodium sulfate 0.994 g, calcium nitrate 0.164 g and sodium chloride 0.012 g were added in 1 L water. The corrosion period of test beam was from October to January. The temperature and humidity were naturally occurring and uncontrolled. In the test, the simulated acid rain solution was controlled to be about 5 cm higher than the steel strand axis by semi-immersion corrosion. During the immersion, the pH value of solution was measured twice a day and it was adjusted to 2.3 by nitric acid.

Basic principle and data processing method of loading experiment

The experimental principle of split Hopkinson compression bar is shown in **figure 4**. The test beam is placed between incidence bar and transmission bar. The bullet is ejected by high pressure gas and then the bullet strikes the incident rod, thus the incident stress wave is formed at the end of incident rod. When the incident wave propagates to the interface between the incident rod and the test beam, due to the difference of wave impedance between incident rod and test beam, some incident waves are reflected back to the incident rod, and the other parts completes the loading of test beam, and they are propagated to the transmission rod (Chen et al. 2020). The incident pulse signal ε_I, the reflected pulse signal ε_R and the transmitted pulse signal ε_T can be recorded by the dynamic strain gauge on the incident bar and the transmission bar. According to the theory of one-dimensional stress wave, the force at both ends of test beam can be determined, and the strain rate of beam in the test can be calculated.

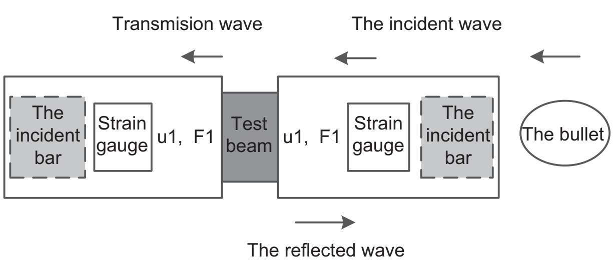

Fig 4. Schematic diagram of split Hopkinson pressure bar impact splitting test.

In the impact splitting experiment, the contact area between incident bar and concrete test beam is very small, and the wave impedance of test beam is low, so most of the incident waves will be reflected back to the incident bar, and the incident pulse signal is close to the reflected pulse signal. Only a small part of the stress wave is propagated to the transmission bar through the test beam. In addition, the transmitted pulse signal is small. The difference between transmitted pulse signal and incident pulse signal is about one order of magnitude.

Because the size of incident pulse signal is very close to the reflected pulse signal, the calculation of the force at the interface between the incident bar and the test beam by incident wave and reflected wave may lead to great error in test result. Therefore, Pan (2022) suggested that the dynamic splitting tensile strength of concrete should be calculated by transmission pulse signal. The formulas are:

$$f_{td} = F_T \Big/ \left(\frac{1}{2} LNG \right) \tag{1}$$

$$F_T = \pi D^2 E_0 \varepsilon_T / 4 \tag{2}$$

In formulas, F_T is the force at the transmission end of concrete beam; f_{td} is the dynamic splitting tensile strength of concrete beam. L is the thickness of test beam. N is the length of test beam. G is the width of test beam. D is the diameter of transmission rod. E_0 is the elastic modulus of transmission rod.

The formula of calculating stress rate $\dot{\sigma}$ and strain rate $\dot{\varepsilon}$ is as follows:

$$\dot{\sigma} = f_{td} / \tau \tag{3}$$

$$\dot{\varepsilon} = \dot{\sigma} / E \tag{4}$$

where, τ is the time when the test beam reaches the transmission peak stress. E is the elastic modulus of concrete beam.

The formulas of calculating the interface displacement u_1 between the incident bar and the test beam and u_2 between the transmission bar and the test beam are shown as follows:

$$\begin{aligned} u_1 &= C_0 \int_0^t \varepsilon_I dt + \left(-C_0\right) \int_0^t \varepsilon_R dt \\ &= C_0 \int_0^t \left(\varepsilon_I - \varepsilon_R\right) dt \end{aligned} \tag{5}$$

$$u_2 = C_0 \int_0^t \varepsilon_T dt \tag{6}$$

In formulas, C_0 is the elastic wave velocity of Hopkinson compression bar.

Determination of corrosion rate of steel strand

After the test beam is loaded, it shall be destructed, and then the steel strand with 60 cm midspan is cut off. After the scum and rust on the surface are cleaned, the mass is measured by an electronic balance with the weighing range of 10 kg and accuracy of 0.1 g, and then above steps should be repeated until the difference is 0.1 g, and the final value is recorded (Chen et al. 2021a). The corrosion rates of steel strands from TYL-a~TYL-h are 3.87%, 0%, 7.22%, 9.84%, 7.12%, 7.24%, 6.71% and 7.42% respectively.

Numerical simulation of micro particle discrete element in concrete corrosion loading experiment

In order to analyze and research the concrete corrosion loading experiment on the meso level, the micromechanics idea is applied to the numerical method of particle discrete element. The concrete micromechanics preprocessing method based on background grid and the inversion technology of meso parameters are used to build the concrete particle discrete element micromechanics model (Watson et al. 2016). Moreover, the meso numerical simulation is performed on the concrete corrosion loading experiment.

Particle discrete element calculation principle and contact constitutive model

In 1979, Cundall and Stack applied the concept of discrete element to the mechanical research of granular materials, thus forming the granular discrete element (Yu et al., 2017). The basic principle is:

1) According to the position and radius of particle element, the contact relationship between the elements is determined. For the elements in contact, the contact force between particle elements is calculated by the contact constitutive model (force-displacement law);
2) According to the contact force calculated in the first step, Newton's second law is used to calculate the acceleration, velocity and displacement of particle element motion, and then the position of particle element and the contact relationship are updated. In this way, the calculation is repeated until the test beam is damaged or the predetermined condition is met.

The linear elastic contact constitutive model is adopted for the force-displacement law, and the formula of calculating contact force is shown as follows:

$$F_n = K_n U_n \tag{7}$$

$$\Delta F_s = -K_s \Delta U_s \tag{8}$$

In the formula, U_i is the contact coincidence (i = n, s); F_i is the contact force; $K_i = k_{i,A} k_{i,B} / (k_{i,A} + k_{i,B})$ is the contact stiffness; $k_{i,A}$ and $k_{i,B}$ are the stiffness of particle elements constituting the contact.

When the particle discrete element is used to calculate the solid mechanics of continuous medium, the contact bond model can be used to bond the particle elements at the contact (Qin et al. 2018). This kind of cohesion has a certain strength. When the normal contact force reaches the normal adhesive strength σ_n, the normal bonding is broken, so it can no longer bear the tensile stress. When the tangential contact force reaches the tangential bond strength σ_s, the tangential adhesive is destroyed, and the tangential movement meets the slip model. When $F_s > F_{s,\max} = \mu |F_n|$, the sliding occurs and $F_s = F_s (F_{s,\max} / |F_s|)$. The calculation model is shown in **figure 5**.

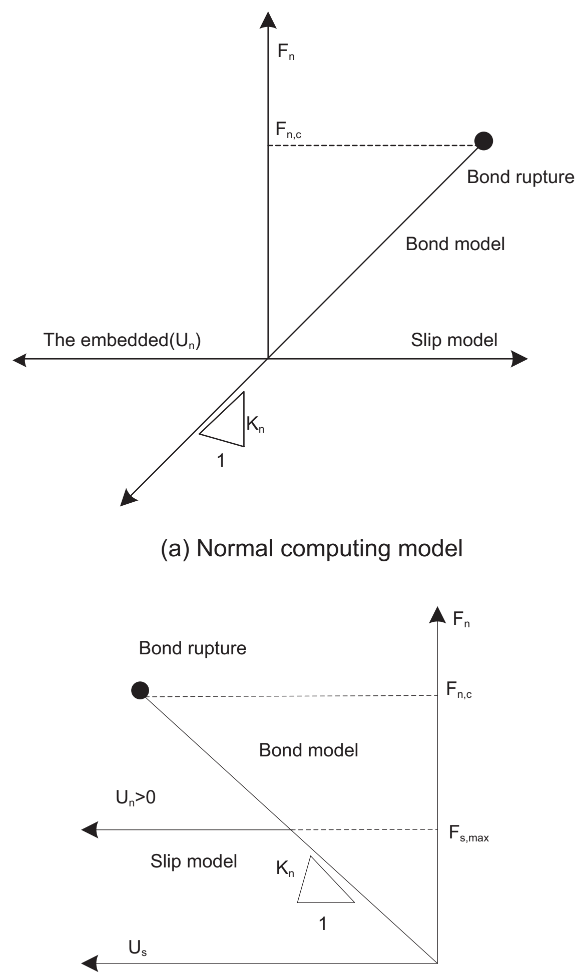

Fig. 5. Contact bonding model and slip model.

Construction of concrete particle discrete element micromechanical model

The concrete micromechanical model is built by following parts: generation of micromechanical model (generation and delivery of random aggregate) and identification of three components (aggregate, mortar, interface) (Hu and Guang 2016). On this basis, a concrete micromechanical preprocessing method based on background grid is proposed, including the aggregate placement and the identification of three components. Compared with the traditional methods, the proposed method improves the preprocessing efficiency and makes the model reach a higher aggregate content. It is widely applied to the pretreatment of concrete micromechanical model. The pretreatment process is briefly introduced as follows.

The aggregate packing process based on the background grid in the pretreatment is shown in **figure 6**.

The main steps and methods of the three-component identification of micro particle discrete element in pretreatment are shown as follows.

1) After the concrete model of particle discrete element is built, we assume that the center coordinate of a discrete particle element is (i, j), then the material properties of a particle element can be determined by following criteria: a) If M_{ij} in the corresponding background grid state matrix is 1, then it is an aggregate element; b) If M_{ij} in the corresponding background grid state matrix is 0, then it is a mortar element. ($M_{ij} = 1/0$ indicates that there is some aggregate or no aggregate at grid point (i, j) in the meso geometric model. After the aggregate packing based on the background grid is completed, the M_{ij} corresponding to each point in space is a given quantity).
2) According to the following criteria, the contact properties between discrete elements are determined: a) If the two small balls involved in contact are aggregate balls, they are aggregate internal contact; b) If the two small balls involved in contact are mortar small balls, they are mortar internal contact; c) If the two small balls involved in contact are aggregate and mortar small balls, they are interface contact.

According to the mix proportion of concrete, the aggregate content of concrete is about 38% (volume percentage). The aggregate diameter is 5-25 mm. The method of concrete micromechanical pretreatment based on background grid is used to randomly place, and thus to form 140 mm × 240 mm micromechanical geometric model and three-component identification. The micromechanical particle discrete element calculation model is shown in **figure 7**.

Experimental device

In this paper, a 74 mm split Hopkinson pressure bar with variable cross-section in the State Key Laboratory of Explosion Science and Technology (Beijing

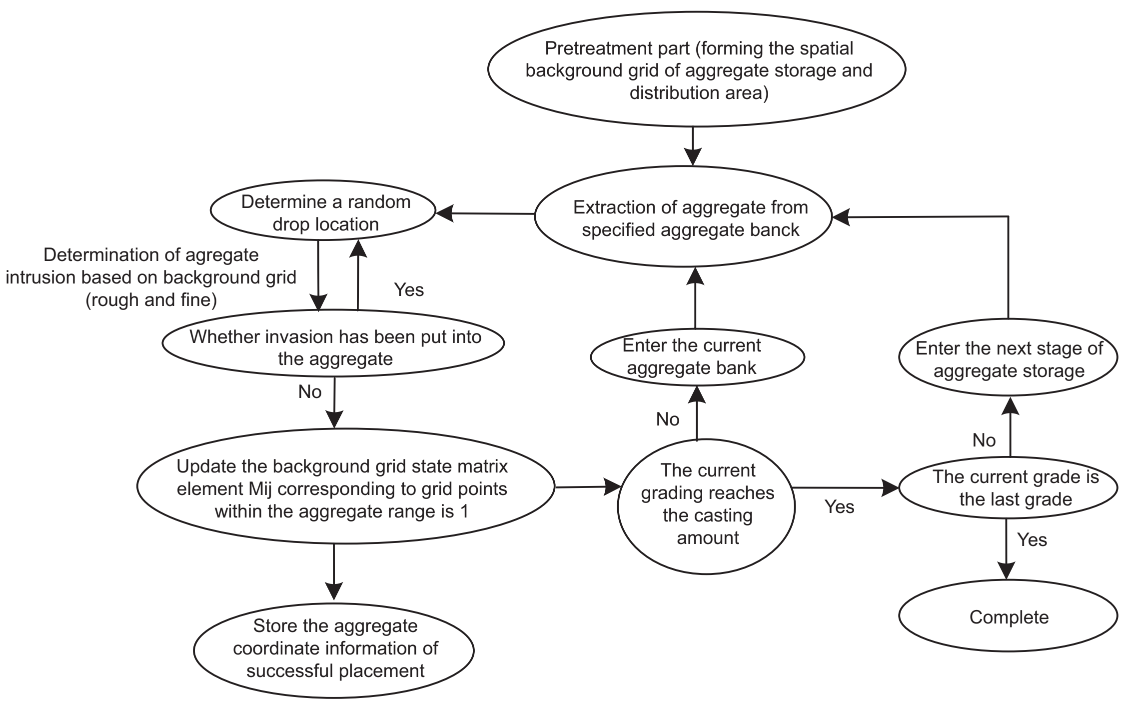

Fig. 6. Process diagram.

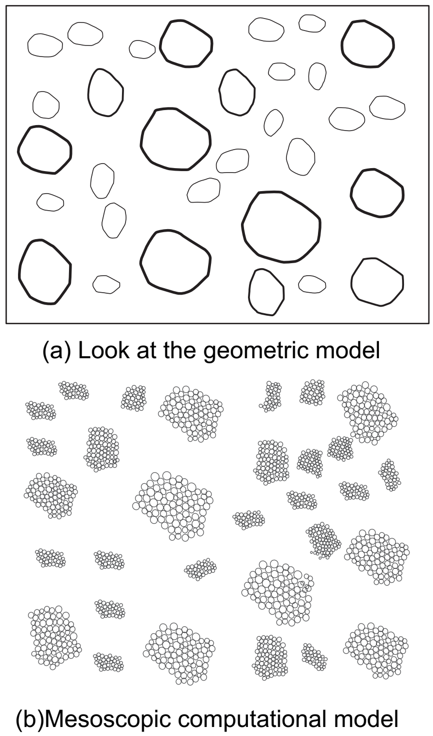

Fig 7. Meso-mechanical model of concrete.

Institute of Technology) was applied in the impact splitting tensile experiment of concrete. The material of incident bar and transmission bar is maraging steel with elastic modulus of 206 GPa. The incident bar is variable cross-section bar with length of 3200 mm. The length of variable cross-section is 400 mm and the diameter is increased from 54 mm to 74 mm. The length of transmission bar is 1800 mm and the diameter is 74 mm.

RESULTS

Through the proposed method, the bending moment-deflection change, load-displacement change and splitting tensile strength change of test beam were obtained. The result of the proposed method was compared with the result of finite element analysis, the result of regression analysis and actual result to verify the accuracy.

Change of bending moment-deflection and load displacement

In order to obtain more reliable experimental results, the experimental results in this paper are the average value of 10 samples. The main test results of the bending moment-deflection of test beam are shown in **Table IV**. The test value of cracking bending moment is M^t_{cr}. The test value of yield bending moment is M^t_y. The test value of ultimate bending moment is M^t_u.f^t denotes the deflection test value of midspan section, $\Delta = f_u / f_y$. The load displacement of test beam classified by the influencing factors such as the concrete strength, the prestressing force and the corrosion rate of steel strand are shown in **figure 8**.

According to the experiment phenomenon of beam and the change of moment-deflection, the stress process can be roughly divided into three stages.

The first stage is the elastic working stage before the cracking of test beam. When the applied load is less than 0.285 M^t_u, the concrete tension area is not cracked, and the bending moment is basically the same as the displacement.

The second stage is the crack stage from the cracking to reinforcement yielding. When the applied load is between 0.285 M^t_u and 0.4 M^t_u. The tensile stress of the concrete at the bottom of the pure bending section

TABLE IV. PURE BENDING TEST RESULTS.

Specimen number	Cracking moment test value/kN/m	Test value of deflection of cracked mid-span section/mm	Yield moment test value/kN/m	Yield mid-span section deflection test value/mm	Limit moment test value/kN/m	Test value of deflection of limit mid-span section/mm	Δ
TYL-a	20.8	1.24	48.4	8.9	56.7	15.5	1.74
TYL-b	19.6	1.56	47.0	9.2	54.9	13.8	1.50
TYL-c	19.0	1.18	45.3	9.4	52.4	13.5	1.44
TYL-d	18.2	1.41	44.1	9.7	49.8	13.9	1.43
TYL-e	18.4	1.40	58.1	10.6	63.4	16.5	1.56
TYL-f	18.1	1.35	63.4	11.0	66.4	14.6	1.33
TYL-g	18.8	1.23	48.4	9.4	54.4	14.9	1.59
TYL-h	16.4	0.87	46.7	10.1	52.3	13.5	1.34

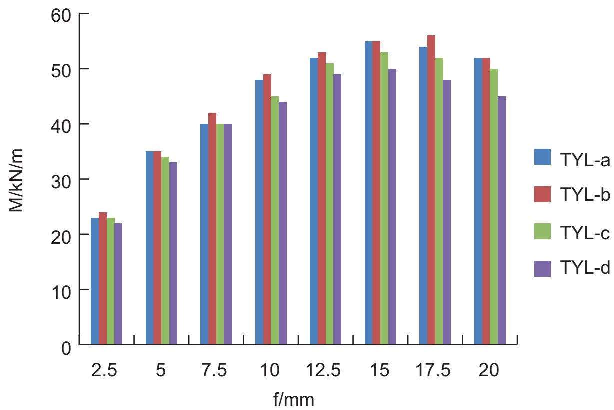

(a) Effect of corrosion rate on load-displacement

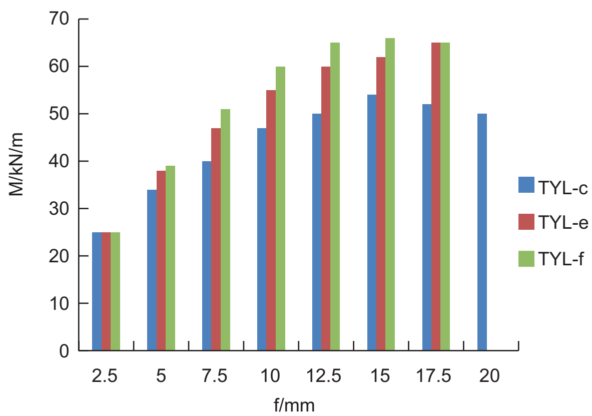

(b) The influence of prestress on load-displacement

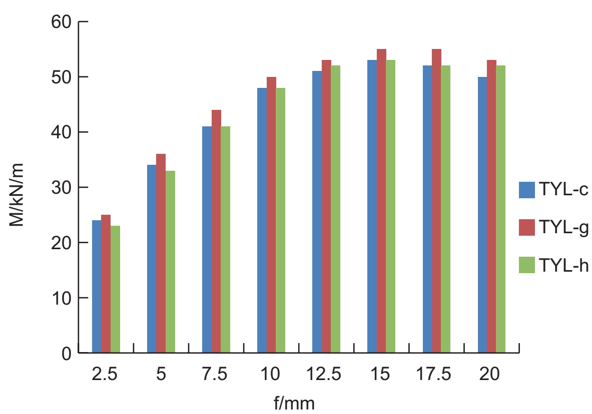

(c) Influence of concrete strength on load-displacement

Fig. 8. Load-displacement variation.

of test beam counteracts the prestress and the tensile strength of concrete provided by the prestressed reinforcement. At first, a vertical micro bending crack appears at the bottom of pure bending section of test beam. At this time, most of the concrete in the compression area stops, and the flexural rigidity of concrete section decreases, and the first point of inflection appears in the load displacement. After that, the load continues to increase, and the crack begins to extend upward. When the crack reaches the reinforcement, the increase of strain reinforcement is suddenly accelerated, and the number of cracks is obviously increased, but the spacing is relatively uniform. The initial width of crack is about 0.05 mm.

The third stage is the failure stage from the yield of reinforcement to the failure of test beam. When the load is 0.8 M_u^t, the reinforcement is yielded and the mid span deflection of test beam increases rapidly. In the failure area, the concrete in compression area forms the horizontal cracks, which is accompanied by the sound of concrete cracking. Finally, the concrete in compression area is crushed or even peeled off. At this moment, the test beam reaches of the ultimate state. The final failure forms of all test beams are the concrete crushing in compression area.

Change of splitting tensile strength

Four grades impact splitting test air pressure are 0.13 MPa, 0.18 MPa, 0.28 MPa and 0.43 MPa. The changes of splitting strength of the test beam with different acid rain corrosion rates are calculated by the proposed method. Based on the calculation results, the influence of acid rain corrosion on the mechanical property of concrete test beam is analyzed. The splitting strength change of test beam is shown in **figure 9**.

According to **figure 9**, we can see that the splitting tensile strength of TYL-b test beam is the highest under different atmospheric pressures in eight concrete beams. The splitting tensile strength of TYL-a beam is second only to TYL-b beam, and the splitting tensile strength of TYL-d beam is the lowest. Other beams are similar in the splitting tensile strength. Therefore, the acid rain corrosion has an impact on the mechanical properties of concrete. The higher the corrosion rate, the lower the splitting tensile strength of concrete. Thus, the acid rain corrosion is inversely related to the mechanical properties of concrete.

Comparison of accuracies

In order to verify the accuracy of analysis results of the proposed method, the result of the proposed method was compared with the result of finite element analysis, the result of regression analysis and the actual splitting tensile strength of test beam. The accuracy comparison is shown in **table V**.

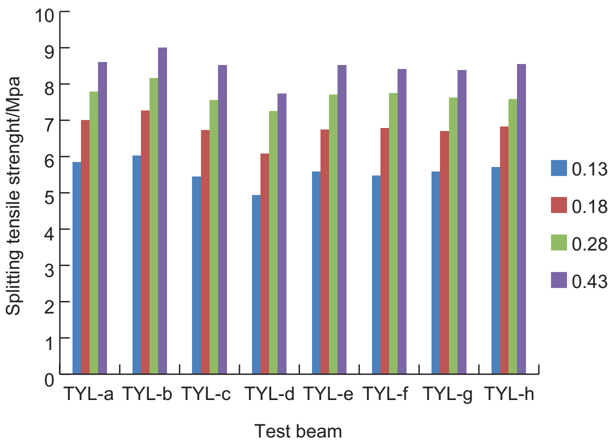

Fig 9. The variation of splitting tensile strength of each test beam.

According to the data in **table V**, we can see that the splitting tensile strength results of test beams obtained by the proposed method are very close to the actual value under the condition of same air pressure change, so the proposed method has high accuracy, and the analysis results are in accordance with the actual situation. Thus, this method can be used to analyze the impact of mechanical properties of concrete after the acid rain corrosion, with high practical application value.

DISCUSSIONS

For the prestressed concrete members in acid rain area, the carbonation rate of concrete is accelerated and the strength of concrete is decreased due to many environmental corrosion factors such as $SO4^{2-}$, NO^{3-}, Cl^{-} and HCO^{3-} in acid rain. In particular, $SO4^{2-}$ not only decomposes the cement stone, but also expands and destroys the concrete due to the reaction of sulfate iron and calcium ion, accelerating the transmission of Cl^{-} in concrete. When the concentration of Cl^{-} around the reinforcement reaches the critical value, the passivation film on the surface of reinforcement is destroyed, and then the corrosion occurs (Ahmed et al. 2019, Dong et al. 2018, Wang et al. 2017). The prestressed reinforcement is brittle than that of ordinary reinforcement. After contacting with corrosive medium, the corrosion occurs rapidly. The time from the beginning of corrosion to failure is very short. The failure form is brittle failure without any foreboding. During the construction of prestressed concrete structure, it is necessary to complete many complex steps, but the quality defects of any step may lead to the corrosion of reinforcement, thus reducing the durability of structure. In the past few years, insufficient durability of prestressed concrete structure leads to many failure accidents of concrete structures, resulting in huge economic losses and human deaths

TABLE V. COMPARISON OF ANALYSIS RESULTS.

Methods	The test pressure/MPa	TYL-a strength / MPa	TYL-b strength / MPa	TYL-c strength / MPa	TYL-d strength / MPa	TYL-e strength / MPa	TYL-f strength / MPa	TYL-g strength / MPa	TYL-h strength / MPa
In this paper, methods	0.13	5.85	6.03	5.45	4.94	5.58	5.47	5.58	5.71
	0.18	7.01	7.27	6.73	6.08	6.74	6.79	6.71	6.83
	0.28	7.79	8.17	7.56	7.26	7.71	7.75	7.62	7.59
	0.43	8.61	9.01	8.52	7.74	8.52	8.41	8.38	8.55
Finite element analysis method	0.13	6.04	6.25	5.31	5.13	5.21	5.21	5.46	5.89
	0.18	6.72	7.48	6.52	6.24	6.53	6.63	6.58	6.51
	0.28	8.15	8.36	7.38	7.11	7.68	7.98	7.33	7.21
	0.43	9.02	9.43	8.74	7.45	8.94	8.12	8.12	8.43
Regression analysis method	0.13	6.45	6.78	5.01	5.68	6.05	6.21	5.03	5.13
	0.18	7.69	7.89	6.22	6.82	7.08	7.52	6.24	6.22
	0.28	8.61	8.94	7.24	6.98	8.32	8.42	7.15	7.06
	0.43	9.54	9.72	8.11	7.13	9.12	9.01	7.86	8.14
Actual strength	0.13	5.82	6.01	5.48	4.93	5.52	5.49	5.62	5.68
	0.18	6.98	7.24	6.75	6.03	6.71	6.81	6.74	6.79
	0.28	7.84	8.12	7.73	7.29	7.75	7.78	7.68	7.63
	0.43	8.63	9.04	8.49	7.71	8.54	8.46	8.35	8.52

(Fikriah et al. 2020, Pasha et al. 2016). Therefore, it is significant to research the durability of prestressed concrete structures in corrosive environment.

CONCLUSIONS

In this article, a method to analyze the influence of mechanical properties of concrete corroded by acid rain based on particle discrete element was proposed. The concrete corrosion loading test was simulated numerically by the micro particle discrete element, and the micro mechanical model of concrete particle discrete element was built. According to the test result, we can see that the cracks of concrete beams corroded by acid rain increase gradually with the increase of load. The corrosion rate of acid rain is inversely proportional to the splitting tensile strength of concrete beams. The results of the proposed method are in accordance with the actual results, so this method has high practical value. In the future, the proposed method will be used to analyze the mechanical properties of prestressed concrete beams in other aspects, and to study the mechanical properties of concrete-filled steel tubular members after acid rain corrosion, so as to further verify the feasibility and analysis effect of the method.

In this article, experimental research and theoretical analysis are combined to analyze the deteriorative characteristics of mechanical properties of prestressed concrete beams in simulated acid rain environment, based on the particle discrete element method. Due to the limitation of experimental time and experimental condition, there are some problems. Therefore, some suggestions are put forward for researchers, mainly including:

1) In this paper, the method of electrified accelerated corrosion is simple, but it is slightly different from the corrosion state of steel strand in natural environment.
2) For the durability of concrete structure in acid rain environment, it is necessary to consider the chemical erosion effect of acid rain on the building and the physical erosion effect on its durability.
3) In this paper, the test belongs to short-term loading, without considering the influence of corrosion on prestressed concrete beams under long-term load.
4) The service life prediction model of prestressed concrete structure in acid rain environment is built by combining accelerated corrosion in laboratory with natural corrosion.

ACKNOWLEDGMENT

The research was supported by the Natural Science Foundation of Shaanxi Province (No. 2018JM5162).

REFERENCES

Ahmed N., Islam M.N., Hasan M.F., Motahar T. and Sujauddin M. (2019). Understanding the political ecology of forced migration and deforestation through a multi-algorithm classification approach: the case of Rohingya displacement in the southeastern border region of Bangladesh. Geology, Ecology, and Landscapes 3, 282-294. https://doi.org/10.1080/24749508.2018.1558025

Aqsa A. (2020). Gully plugging spillway is an effective gully rehabilitation measure: a case study of district Gujrat-Pakistan. Big Data in Water Resources Engineering 1, 6-9. https://doi.org/10.26480/bdwre.01.2020.06.09

Aunsary M.N. and Chen B.C. (2019). Sustainable water treatment management. Water Conservation and Management 3, 11-13. https://doi.org/10.26480/wcm.02.2019.11.13

Chen F.X., Jin Z.Q., Wang E.D., Wang L.Q., Jiang Y.D., Guo P.F., Gao X.Y. and He, X.Y. (2021a). Relationship model between surface strain of concrete and expansion force of reinforcement rust. Scientific Reports 11, 4208. https://doi.org/10.1038/s41598-021-83376-w

Chen F.X., Zhong Y.C., Gao X.Y., Jin Z.Q., Wang E.D., Zhu F.P., Shao X.X. and He X.Y. (2021b). Non-uniform model of relationship between surface strain and rust expansion force of reinforced concrete. Scientific Reports 11, 8741. https://doi.org/10.21203/rs.3.rs-135397/v1

Chen M.C., Fang W. and Huang H. (2020). Study on static performance of concrete filled steel tube (CFST) members simulated by acid rain. Engineering Mechanics 2, 43-52. https://doi.org/10.21203/rs.3.rs- 135397/v1

Dong L., Liu J. and Xiu L.D. (2018). A theoretical method to determine the tortuous crack length and the mechanical parameters of concrete in direct tension-A particle size effect analysis. Engineering Fracture Mechanics 197, 128-150. https://doi.org/10.1016/j.engfracmech.2018.04.039

Fikriah F., Kamaruzzaman Y., Mohd Fuad M. and Azman A. (2020). Assessment of trace metals using chemometric analysis in Kuantan River, East Coast Malaysia. Journal Clean WAS 4, 1-7. https://doi.org/10.26480/jcleanwas.02.2019.01.04

Hao J.F., Dao C.G. and Jian, C.D. (2017). Discrete element method simulation of the mixing process of particles with and without cohesive interparticle forces in a fluidized bed. Powder Technology 327, 223-231. https://doi.org/10.1016/j.powtec.2017.12.016

Hu Q.Q. and Guang S. (2016). Preparation and properties of high strength physical-chemical hybrid double-network hydrogels. Journal of Jilin University (Science Edition) 54, 1146-1151. https://doi.org/10.13413/j.cnki.jdxblxb.2016.05.36

Kaianauskas R., Maknickas A. and Markauskas D. (2015). Adapting the discrete element method to simulation of acoustic agglomeration of aerosol particles. AIP Conference Proceedings 1648, 400006. https://doi.org/10.1063/1.4912626

Kang L., Du H.L., Du X., Wang H.T., Ma W.L., Wang M.L. and Zhang, F.B. (2018). Study on dye wastewater treatment of tunable conductivity solid-waste-based composite cementitious material catalyst. Desalination and Water Treatment 125, 296-301. https://doi.org/10.5004/dwt.2018.22910

Michael A.F., Leigh W. and Mohamed A.B. (2016). Shielding properties of protective thin film coatings and blended concrete compositions for high level waste storage packages. Annals of Nuclear Energy 89, 63-69. https://doi.org/10.1016/j.anucene.2015.11.026

Pan J.W., Zhong W., Wang J.T. and Zhang C.H. (2022). Size effect on dynamic splitting tensile strength of concrete: Mesoscale modeling. Cement and Concrete Composites 128(9), 104435. https:https://doi.org/10.1016/j.cemconcomp.2022.104435

Pasha M., Hare C. and Ghadiri M. (2016). Effect of particle shape on flow in discrete element method simulation of a rotary batch seed coater. Powder Technology 298, 29-36. https://doi.org/10.1016/j.powtec.2015.10.055

Qin Z., Xiao J.W. and Liang, X. (2018). Waterlogging and simulated acid rain after anthesis deteriorate starch quality in wheat grain. Plant Growth Regulation 85, 257-265. https://doi.org/10.1007/s10725-018-0390-8

Wang Q., Liu Y. and Peng G. (2017). Water content in concrete under water pressure environment and the effect on its mechanical properties. Journal of Hydraulic Engineering 48, 193-202. https://doi.org/10.13243/j.cnki.slxb.20160539

Watson N.J., Povey M.J.W. and Reynolds G.K. (2016). Development of a discrete element model with moving realistic geometry to simulate particle motion in a mi-pro granulator. Computers & Chemical Engineering 93, 234-247. https://doi.org/10.1016/j.compchemeng.2016.06.021

Yu P.X., Jordan M. and Ting W.L. Particles climbing along a vertically vibrating tube: numerical simulation using the Discrete Element Method (DEM). Powder Technology 320, 304-312. https://doi.org/10.1016/j.powtec.2017.07.047

Zhang K.K., Ma W.W. and Jiang W. (2020). Study on mechanical properties of Nano-SiO_2 modified concrete based on digital image technology. Nanotechnology 4, 10-15. https://doi.org/10.1016/10.12677/NAT.2020.104008

Zohdi T.I. (2016). A discrete element and ray framework for rapid simulation of acoustical dispersion of microscale particulate agglomerations. Computational Mechanics 57, 465-482. https://doi.org/10.1007/s00466-015-1250-2